Research Square

Preprints are preliminary reports that have not undergone peer review.
They should not be considered conclusive, used to inform clinical practice,
or referenced by the media as validated information.

Centrifugal force driven low frequency modes in a spherical tokamak

G. Z. Hao

haogz2019@outlook.com

Southwestern Institute of Physics

G. Q. Dong

Southwestern Institute of Physics

Y. Q. Liu

General Atomics

W. W. Heidbrink

University of California

S. Xu

Southwestern Institute of Physics

E. D. Fredrickson

Princeton Plasma Physics Laboratory

J. Berkery

Princeton Plasma Physics Laboratory

S. Munaretto

Princeton Plasma Physics Laboratory

K. F. Gan

University of Tennessee

W. L. Zhong

Southwestern Institute of Physics

Article

Keywords:

Posted Date: November 13th, 2026

DOI: https://doi.org/10.21203/rs.3.rs-11251918/v1

License: This work is licensed under a Creative Commons Attribution 4.0 International License.
Read Full License

Additional Declarations: No competing interests reported.

Centrifugal force driven low frequency modes in a spherical tokamak

G.Z. Hao[1,+*], G.Q. Dong[1,+], Y.Q. Liu[2], W.W. Heidbrink[3], S.Xu[1], E.D. Fredrickson[4], J. Berkery[4], S. Munaretto[4], K.F. Gan[5], and W.L. Zhong[1]

[1]*Southwestern Institute of Physics, Chengdu 610041, China*

[2]*General Atomics, San Diego, California 92186, USA*

[3]*University of California, Irvine, California 92697,USA*

[4]*Princeton Plasma Physics Laboratory, Princeton, New Jersey 08540, USA*

[5]*University of Tennessee, Knoxville, Tennessee,37996, USA*

Abstract

The physics nature of a low frequency (<50 kHz) core-located magnetohydrodynamic (MHD) instability, observed at the early phase of discharges on the National Spherical Torus Experiment (NSTX) (Ono *et al 2000 Nucl. Fusion* **40** 557), has been a longstanding puzzle. Rapid plasma flow is found to be the drive for these low frequency modes in spherical tokamaks (ST). In particular, the centrifugal force is identified as the key physics mechanism for triggering the instability. Toroidal modeling explains the observed mode frequency, the mode internal structure, as well as the threshold flow value for the instability onset. Futhermore, the dominant poloidal mode number is identified as $m = 2$ for the first time. These results are highly relevant to ST-based fusion reactor design for avoiding fast-flow driven core MHD instabilities.

[+]These authors contributed equally to this work.

[*]Email: haogz2019@outlook.com

Introduction.— Spherical tokamaks (ST) are attractive magnetic configuration devices for developing fusion energy [1, 2]. It is well known that toroidal rotation can ameliorate or suppress many performance-limiting magneto-hydrodynamic (MHD) instabilities, such as resistive wall modes [3, 4] and tearing modes [5], in magnetic confinement fusion devices. However, excessively fast plasma flows can drive MHD instabilities, such as the Kelvin-Helmholtz (KH) instability[6], which consequently degrades plasma performance. Furthermore, centrifugal forces associated with fast toroidal flow of the plasma can drive a kind of interchange-like instability [7, 8]. Owing to the small plasma volume per unit of Neutral Beam Injection (NBI) power, ST plasmas can rotate toroidally at a significant fraction of the Alfvén speed [9]. This letter reports conclusive identification of the role of centrifugal force in driving a class of low frequency internal instabilities in an ST - the National Spherical Torus Experiment (NSTX) [10, 11]. This type of instability is likely to occur in some future ST designs, such as the Component Test Facility (ST-CTF) [1], in which the plasma Alfvén Mach number is ~ 0.4, comparable to the value on NSTX. The results presented in this work may help ST-CTF avoid instabilities driven by fast flow, such as through controlling the density profile to mitigate the centrifugal force in the core plasma region. In addition to the importance for STs, MHD instabilities driven by fast flow or flow shear are common and play important roles in naturally occurring plasmas. For instance, KH instability driven by sheared flows [12] was utilized to explain the anomalous transport in the solar-wind magnetosphere [13], as well as to account for the source of inhomogeneous mixing elements in nova explosions [14].

Low frequency (< 50 kHz) instabilities are often observed in the early phase of NSTX discharges [15]. The frequency of the instability typically matches well the plasma toroidal rotation frequency at the radial location of the mode, which is usually within a major radius of $R < 120$ cm. At the saturated state, this kind of mode induces a drop of the neutron rate by $\sim 20\%$ [16], a drop of beam-driven current by $\sim 40\%$ [16] and a toroidal beta (β_T) drop by $\sim 7\%$ [16, 17]. Here, $\beta_T \equiv 2\mu_0 < p > /B_T^2$ is the volume averaged dimensionless plasma pressure. The fast-ion redistribution and the accompanied beam-driven current are sensitive to the mode structure of the instability [16]. Therefore, in order to precisely simulate the plasma performance affected by this kind of instability, it is important to identify the onset conditions.

Characteristics of the mode evolution after mode onset are extensively studied. For

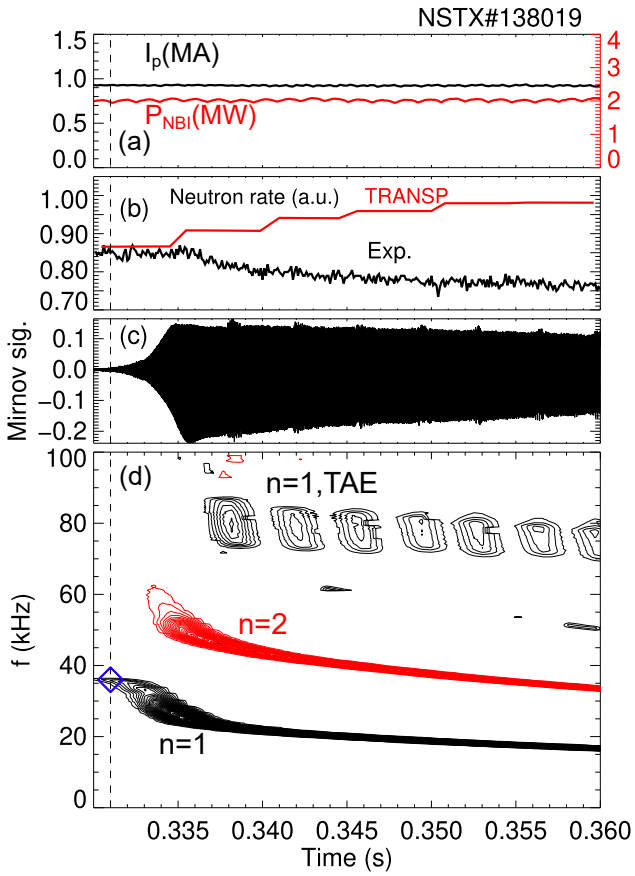


FIG. 1. Time traces of the NSTX discharge 138019 with (a) the plasma current and NBI heating power, (b) the measured(black) and predicted(red) neutron rate, (c) the raw data and (d) spectrum of the Mirnov signal. Dashed line denotes the onset time of the n=1 low-f mode, with symbol $'\Diamond'$ indicating the plasma rotation frequency at R=116 cm before the mode onset.

example, the dependence of bifurcations of mode frequency on the evolution of $q-$ profiles is figured out in [15]. Effect of a kind of low frequency mode with assuming a kink-tearing structure on the fast ion redistribution is studied in [18]. The $m/n = 1/1$ internal mode structure after the mode onset are studied in [11].

However, there has been a longstanding debate about what causes the onset of this instability. Here, we identify the fast flow induced centrifugal force as the key driving mechanism for this class of instability.

Experimental observation.— A typical discharge of NSTX, with the machine major radius of $R_0 = 0.85$ m and the plasma minor radius of $a = 0.65$ m, operates at the toroidal magnetic field of $B_T \leq 0.55$ T and the plasma current I_p up to 1.5 MA. The beam heating

power P_{NBI} is up to 6 MW.

Figure 1 shows an example of an NSTX discharge at plasma current of $I_p = 0.9$ MA and with $P_{NBI} = 2$ MW [Fig. 1(a)]. An $n = 1$ low frequency (low-f) mode occurs at 331 ms [Fig. 1(c-d)]. Here, n is the toroidal mode number. The onset mode frequency matches the plasma toroidal rotation frequency measured at $R = 116$ cm (the magnetic axis position is $R_0 = 101$ cm). During the frequency decay phase of the $n = 1$ mode, an $n = 2$ perturbation also develops. In the saturation phase, the neutron rate is significantly reduced compared to that predicted by the TRANSP simulation [Fig. 1(b)], calculated without any anomalous diffusion for fast ions [19]. Meanwhile, $n = 1$ toroidal Alfvén eigenmode (TAE) bursts also appear. Both the neutron rate change and TAE excitation suggest that the saturated (both n=1 and 2) low-f modes substantially redistribute fast ions. Furthermore, Refs. [16, 20], where the mode structure was approximated by a simple analytical model, also reported that this class of low-f mode enhances the fast ion loss.

Based on the selection criteria that the onset mode frequency matches the plasma rotation frequency at a certain radial location and the identified mode position is located in the core region, a database is established in which $\beta_N = 2 - 5, P_{\rm NBI} = 1.8 - 6$ MW and the toroidal rotation at R_0 varies between 25-45 kHz. Here, $\beta_N \equiv \beta_T a B_T / I_p [\%\mathrm{mT/MA}]$ is the normalized beta. The low-f mode significantly damps the plasma core rotation[21], with one example shown in Fig. 2(a). The process occurs within ~ 10 ms time interval. Outside the core, the plasma rotation slightly increases. Analysis of the database shows that the damping of the core rotation is a generic feature [Fig. 2(c)]. The database also indicates that the radial location of the mode, identified by matching the mode frequency to the plasma rotation frequency, is localized in the core region, near $R = 115$ cm [dashed curve in Fig. 2(b)]. At the mode's radial location, the centrifugal force ($\propto \partial(\rho\Omega^2)/\partial R$), estimated at a time slice just before the observed mode onset, is also relatively large [Fig. 2(d)]. This provides the first indication of the role of the centrifugal force on the mode onset.

Modeling framework.—In order to gain a better physics understanding of the role of the centrifugal force on the $n = 1$ low-f mode, we employ the full toroidal MHD eigenvalue code MARS-F [22, 23]. The code includes, among other physics, plasma toroidal flow as well as plasma resistivity. MARS-F interfaces with a static toroidal equilibrium solver CHEASE [24], which in turn utilizes results from the equilibrium fitting code LRDFIT [25]. LRDFIT assumes an inductance-resistance 2D axisymmetric circuit model for the tokamak

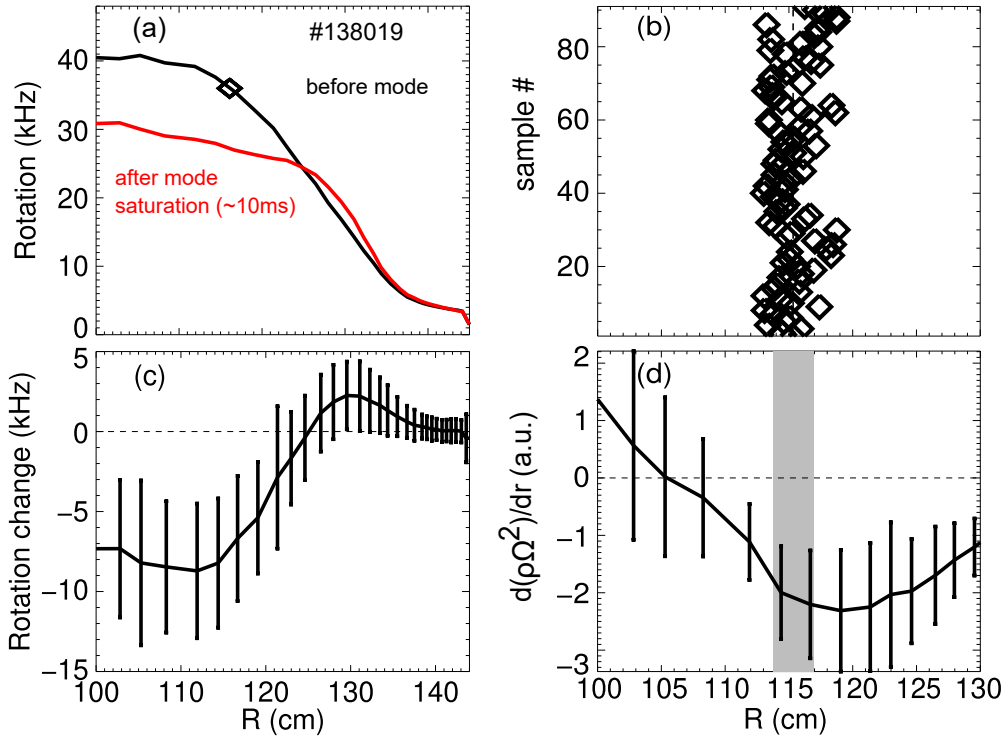


FIG. 2. (a) Plasma toroidal rotation frequency before (black) and after(red) the low-f mode onset in discharge 138019, with $'\diamondsuit'$ labeling the mode frequency at onset. (b) Symbols denote the radial position where the mode frequency matches the plasma rotation frequency, for conditionally chosen 92 NSTX discharges. (c) The low-f mode induced change of rotation and (d) an indicator of the centrifugal force, averaged over shots in the database. In (d), the shaded region denotes the mode location. Error bars in (c) and (d) denote the standard derivation.

equilibrium reconstruction, where the Grad-Shafranov equilibrium is enforced and is constrained to fit to various diagnostic data. In this work, the experimental constraints include the magnetics data, plasma toroidal rotation and motional stark effect (MSE) including electric potential correction.

MARS-F solves, among other MHD equations, the following perturbed momentum equation

$$\begin{aligned}\rho(\gamma+i\omega_r-in\Omega)^2\boldsymbol{\xi} = &-\nabla p+\boldsymbol{j}\times\boldsymbol{B}+\boldsymbol{J}\times\boldsymbol{Q}\\ &+2\rho(\gamma+i\omega_r-in\Omega)\Omega\hat{\boldsymbol{Z}}\times\boldsymbol{\xi}-R\hat{\boldsymbol{R}}\nabla\cdot(\rho\Omega^2\boldsymbol{\xi})\end{aligned} \tag{1}$$

where γ and ω_r are the mode growth rate and real frequency, respectively. ρ, $\boldsymbol{B}$ and $\boldsymbol{J}$ are the equilibrium density, magnetic field and plasma current, respectively. Ω is the plasma toroidal rotation frequency. $\boldsymbol{\xi}$, p, $\boldsymbol{j}$ and $\boldsymbol{Q}$ are the plasma displacement, perturbed

pressure, current and magnetic field, respectively. The unit vectors along the major radius and the vertical direction are $\hat{\boldsymbol{R}}$ and $\hat{\boldsymbol{Z}}$, respectively. The mode toroidal number $n = 1$ is considered in computations. The two inertial terms, $\boldsymbol{F}_{cl} \equiv 2\rho(\gamma + i\omega_r - in\Omega)\Omega\hat{\boldsymbol{Z}} \times \boldsymbol{\xi}$ and $\boldsymbol{F}_{cf} \equiv -R\hat{\boldsymbol{R}}\nabla \cdot (\rho\Omega^2\boldsymbol{\xi})$, represent the Coriolis and centrifugal forces, respectively [26]. In the results reported below, all the frequencies are normalized by the Alfvén frequency $\omega_A \equiv 1/\tau_A$, with τ_A being the toroidal Alfvén time at the magnetic axis.

Key results.— In the following, we report key results of comparing the MARS-F modeling with experiments for (i) the rotation threshold $\Omega_c\tau_A$ for driving the low-f mode, (ii) the onset mode frequency, and (iii) the internal structure of the mode.

We pay special attention to various uncertainty and sensitivity issues in the mode identification. An important uncertainty in the equilibrium reconstruction is the lack of constraint on the pressure profile in LRDFIT, resulting in uncertainty in the reconstructed safety factor profile and uncertainty of the predicted β_N. Furthermore, we also study the dependence of the results on an uncertainty in the measured plasma core density profile. Finally, other physics effects in addition to the centrifugal force in the stability model, such as the plasma resistivity and the drift kinetic effect of fast ions, are also discussed.

Figure 3 reports several examples of the MARS-F computations for an NSTX discharge #137617 at 330 ms, and compares with the experimental results. In these computations, the uncertainty of safety factor profile is considered. The reason for choosing this shot is because the reflectometer data can be applied to identify the mode structure for plasma edge to the the middle region (i.e. $\sqrt{\psi_p} = 0.5$). ψ_p is the normalized poloidal flux.

By specifying different basis functions for the pressure gradient [25] in LRDFIT (while still applying the MSE and other data constraints), slightly different q-profiles are obtained in the plasma core, as shown by the solid curves in Fig. 3(a). The sensitivity study is expanded by including one more case (dash-dotted curve in Fig. 3(a)) with rescaled $q_{\min}$, based on the case labeled 'QP1' with $q_{\min} = 2.1$. The measured density and rotation profiles (Fig. 3(b)) are utilized in MARS-F computation. The uncertainty of measured density is $\sim 4\%$. Here, the experimental data are mapped to flux surface coordinate based on the equilibrium constructed by LRDFIT.

Figure 3(c) shows that, with various choices of q-profiles, an $n = 1$ instability always occurs when the plasma rotation frequency exceeds a critical value $\Omega_c\tau_A$. Here, the measured rotation profile is used, with the amplitude scanned. This shows a robust drive of the

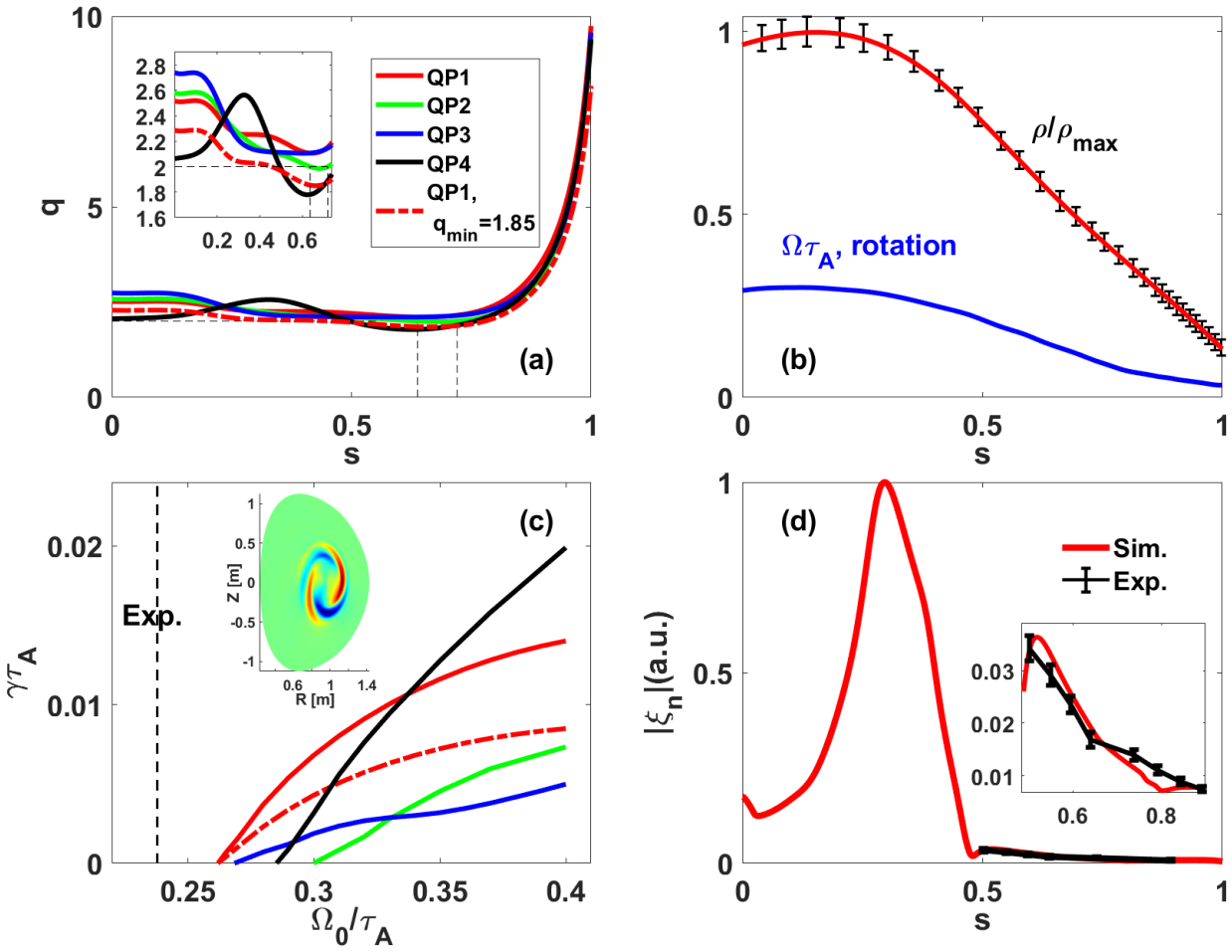


FIG. 3. MARS-F modeling input and results for a discharge #137617 at 330 ms, with (a) the reconstructed (solid) and rescaled (dash-dotted) safety factor profiles,(b) the measured ion density profile normalized to its maximum ρ_{max} (black curve) and the fitted one used in computation (red). The blue curve is the experimental rotation profile. (c) The mode growth rate with varying amplitude of toroidal rotation frequency $\Omega_0\tau_A$ and with different q-profiles as shown in (a). Inserted plot in (c) is an example of the real part of the computed displacement in the (R,Z)-domain for QP1. Shown in (d) is the computed normal displacement (red) together with that reconstructed from the reflectometer data (black). Here, $s \equiv \sqrt{\psi_p}$ with ψ_p being the normalized poloidal flux.

instability against uncertainties in determining the core q-profile. On the other hand, the critical value $\Omega_c\tau_A$ does depend on the q-profile. However, $\Omega_c\tau_A$ almost does not depend on $q_{\min}$ when the q-profile is fixed. It should be noted that the later evolution of these modes have been shown to be influenced by the evolvution qmin value, as presented in [15].

For QP1 case, the corresponding $\Omega_c\tau_A$ value is 0.26, which is close to the measured normalized plasma rotation frequency (0.23) just before the $n = 1$ mode onset. The computed mode frequency (0.24) roughly agrees with the experimental value (0.22). When the density profile used in computation is varied in the uncertainty region of the measurement, the predicted $\Omega_c\tau_A$ value can cover the measured value (0.23). Overall, taking into account the variations in the q-profile, the computed linear stability threshold exceeds the observed value by $\leq 25\%$. Furthermore, it was found that the plasma pressure β_N destabilizes the mode and an increase of β_N by 10% induces a decrease of threshold value $\Omega_c\tau_A$ by 4%. In addition, the Coriolis force has a stabilizing effect on the mode driven by the centrifugal force.

The inserted plot in Fig. 3(c) indicates that the dominant poloidal mode number is $m = 2$ and the perturbation is localized in the core region. In fact the mode peaks at $s = 0.3$ [Fig. 3 (d), for the case of 'QP1' with $\Omega_0\tau_A = 0.3$], being far away from the $q_{min}(= 2.1)$ position of s=0.66. This shows that the mode here is different from the infernal mode, which is often localized at local minimum of q and when q_{min} is sufficiently close to an integer [27, 28].

The shape of the modeled displacement along the mid-plane agrees with the reflectometer data [Fig. 3(d)],which are available only on the outboard side of the plasma column in the studied discharge. It is experimentally confirmed that the perturbation near the edge is very weak, and becomes stronger towards the inside of the plasma. We also mention that the mode peaks at $s \approx 0.3$ for all cases shown in Fig. 3(a).

The radial location of the computed internal mode depends sensitively on the density profile [Fig. 4]. Here, we fix the plasma rotation profile as well as the amplitude ($\Omega_0\tau_A = 0.3$), while the density profile is varied. It is evident that the mode is located at the location of sharp density gradient. The mode frequency, not shown here, follows the local plasma rotation at the mode location. Here, the q-profile is kept the same for different cases shown in Fig. 4. The results thus show that the density profile plays the dominant role on the mode location. Furthermore, additional computations suggest that the other inertial effects (such as the Coriolis force) in addition to the centrifugal force also have contributions to determine the exact mode position. In addition, the critical rotation frequency, $\Omega_c\tau_A$, decreases as the density gradient increases (roughly equivalent to the increase of the centrifugal force) near the mode location. It is pointed out again, when the plasma rotation exceeds a critical value, a kind of $m/n = 2/1$ mode appears, which is insensitive to q profile. The mode structue

peaks near the sharp density gradient.

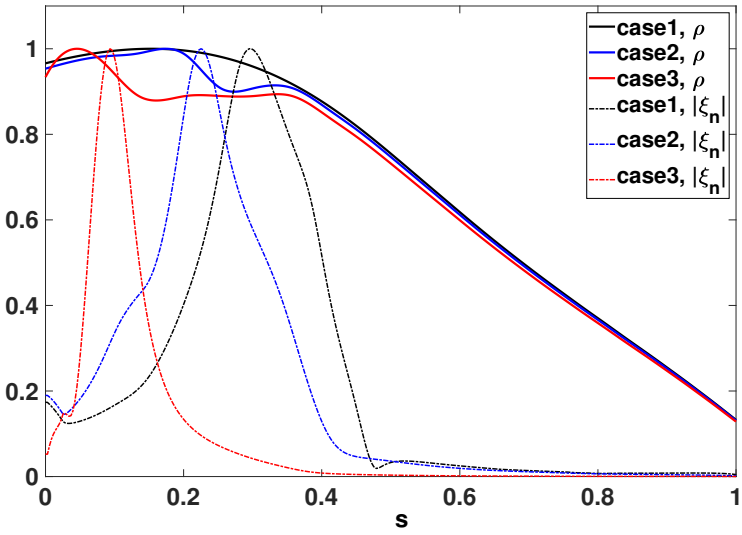


FIG. 4. Plot shows the computed normal displacement (dash-dotted curves) for three choices of the normalized plasma core density profile. The displacement amplitude is arbitrarily rescaled. Considered here is the NSTX discharge #137617.

In order to validate the mode structure in the plasma core region, we utilize Ultra-soft X-ray (USXR) data [18, 29]. The MARS-F computed plasma displacement is used to synthesize the numerical USXR signal, to be compared with the direct measurements. Since there are no USXR data available for discharge #137617, we choose a similar discharge #138019. The modeling predicted critical value of driving low-f mode is about $\Omega_c\tau_A \simeq 0.25$, which is close to the measured plasma rotation frequency $\Omega_c\tau_A \simeq 0.24$ before the mode onset at 331 ms. Again, the behavior of driving low-f mode is insensitive to the constructed q-profile. The reconstructed $q-$profile has a reversed magnetic shear in the core region with $q_{min} >\sim 2.08$. The $q = 2$ resonance surface is also not necessary for the occurrence of low-f mode in shot #138019.

The USXR emission mainly depends on the electron density n_e, temperature T_e and the impurity density n_c. The USXR signal, produced from equilibrium emission, is line-integrated along the line of sight l, as $S_0 = \int \epsilon_0(\psi_p)dl$ with $\epsilon_0 = n_e n_c f(T_e)$. Here, $f(T_e)$ is a weighting function, which is tuned to best match the simulated S_0 profile with the measurements Fig. 5(a). The USXR fluctuation, associated with the mode perturbation, is then represented as $S_1(t) = \int \delta\epsilon_0(\psi_p, \theta, t)dl = \int \mathrm{Re}(e^{i\omega_r t}\boldsymbol{\xi}\cdot\nabla s)\partial\epsilon_0(\psi_p)/\partial s dl$. The perturbation

$\delta\epsilon_0(\psi_p, \theta, t = 0)$ is plotted in Fig. 5(b), together with the geometry of the USXR chords in NSTX.

To simulate the USXR fluctuation, we use the computed mode structure with growth rate $\gamma\tau_A = 4.2 \times 10^{-3}$, which is comparable to the experimental value of $\gamma\tau_A = 6.2 \times 10^{-3}$ at 332 ms. This is the time slice when the USXR fluctuation is extracted from measurements. A key observation is that the simulated integrated USXR fluctuation S_1 exhibits an inversion near chord #5 [Fig. 5(d)], again consistent with the measurements [Fig. 5(c)]. Moreover, the simulated spectrum between chords 1-4 and chords 7-9 also agrees well with the measurements. Along the outer chords #10-15, both the simulated and measured USXR fluctuations are very weak (hence not plotted here). We also point out that the simulated USXR fluctuations using mode structures with much lower or much larger growth rates agree poorly with measurements. This is largely due to the fact that the mode structure becomes narrower (broader) as the growth rate decreases (increases). Another interesting finding is that the simulated inversion radius is fully determined by the radial location of the mode. Figure 5 thus provides convincing evidence for the positive identifications of the core structure of the mode.

We should also point out that the simulated USXR signal at chord #5 (#6) is relatively stronger (weaker) as compared to the measurements. This is possibly due to the uncertainty associated with the weighting function $f(T_e)$.

Discussion.— The ideal MHD modeling results presented so far provide quantitative identification of the $n = 1$ low-f internal instability in the NSTX experiments. We also examined the effect of plasma resistivity and the kinetic effects of particles on the mode onset. The plasma resistivity hardly affects the mode onset here.Non-perturbative, MHD-kinetic hybrid computations using the MARS-K code [30] show that the drift kinetic effects from fast ions lead to very minor change of the mode stability because of the lack of strong resonances as shown in Fig. 6. For fast ions, the wave-particle resonance can occur in the trapping region and near the boundary between the trapping and passing regions. However, in the phase space domain where the resonance is possible, the deposited fast ion density is very low. The fast ions are predominantly deposited in the passing region. Since the mode frequency in the plasma frame, in the $R = 100 - 120$cm radii, roughly varies between -5 and 5 kHz, we consider three mode frequencies (-5, 0, 5) kHz and find that the resonance between the fast ions and the mode is very weak. However, it is mentioned that in some

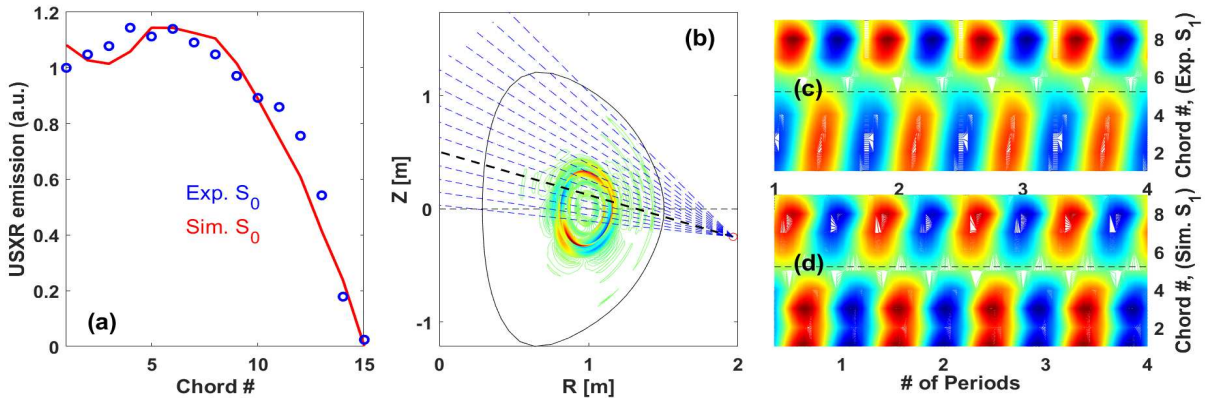


FIG. 5. Comparison of (a) the experimental (blue) and simulated (red) USXR signal from the equilibrium emission ϵ_0. (b) The simulated USXR fluctuation $\delta\epsilon_0$ plotted together with the USXR geometry (dashed lines). (c) The measured and (d) simulated line-integrated USXR fluctuation, in which 'Period' means a period of the oscillation of USXR fluctuation as a function of time. Considered here is the NSTX discharge #138019 at 332 ms.

NSTX discharges with relatively high β_N (~ 3.5) with $q_0 <\sim 2$, the low frequency mode is identified as ideal wall mode [31] at mode onset, where the kinetic effect from fast ions is significant for the appearance of low frequency mode. .

The modeling results reported have so far neglected flow modification to the plasma equilibrium. On the other hand, due to the centrifugal force induced by fast flow, the equilibrium plasma density is no longer a flux function. This introduces a finite equilibrium density/pressure gradient along the poloidal angle of the magnetic flux surface [11]. Recently, the MARS-K code has been updated to include modification to the density/pressure, while the equilibrium temperature is assumed to still be a function of the magnetic flux. In the presence of toroidal rotation, the density profile is modified as $\rho = \rho_s(\psi)\ \exp[\Omega^2(R^2 - R_0^2)/(\Omega_s^2 R_0^2)]$ [32]. Here, $\Omega_s = \sqrt{2T_i/(m_i R_0^2)}$ with T_i and m_i being the ion temperature and mass, respectively. ρ_s is the density profile in the static equilibrium. The pressure profile follows a similar modification.

The computational results based on the new version of MARS-K code generally show validity of the key conclusion reported earlier assuming static equilibria. The mode is still mainly driven by the centrifugal force, with the growth rate computed as $\gamma\tau_A = 3 \times 10^{-2}$ assuming $\Omega = 0.24\omega_A$ and including both aforementioned flow-correction to the equilibrium and drift-kinetic effects of thermal particles. Without showing details, we highlight the

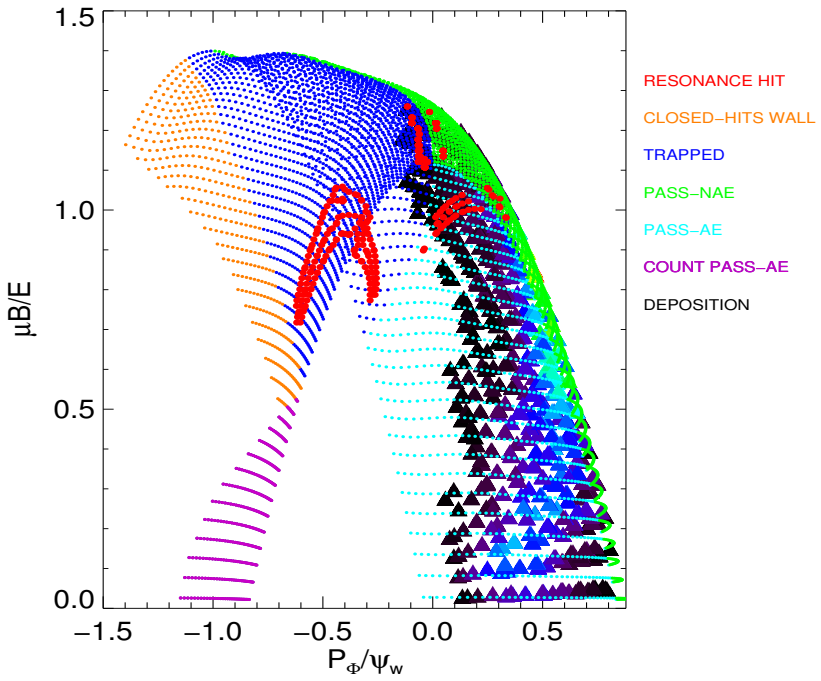


FIG. 6. The resonance condition (red •, labeled by "RESONANCE HIT") between the low-f internal mode and fast ions in the particle phase space. The fast ion energy is fixed at 75 keV. The following aspects are considered: (i) both the toroidal and poloidal frequencies of fast ions are computed; (ii) chosen are three mode frequencies, 0, -5 kHz and 5 kHz, in the plasma frame; (iii) for dumping fast-ion density (▲) from TRANSP computations, the spatial region is limited to $0 < s = \sqrt{\psi_p} <\sim 0.5$, being roughly the mode occupation region. Here, the fast ion peak density is normalized to unity, with black color denoting the relative level <5%. Here, "AE" and "NAE" denotes the orbits that do and do not enclose magnetic axis, respectively. "CLOSED-HITS WALL" denotes the orbits that hit the wall.

following key findings. (i) Within the fluid model, incorporating centrifugal modifications to the equilibrium density/pressure leads to a strong stabilization of the computed mode, which is inconsistent with experimental observations. (ii) In contrast, the self-consistent MHD-kinetic hybrid computation using MARS-K, applied to the same flow-modified equilibrium, recovers the instability. (iii) The essential reason is that the drift-kinetic model, which fully replaces the compressibility term in the fluid model, provides a better physics description of the effect from the parallel motion of thermal particles. The latter appears to be critical to

correctly capture the underlying physics in fast-flowing plasmas.

More importantly, the modeled mode structure (Fig. 7(a)) agrees reasonably well with that (Fig. 7(b-c)) constructed from the experimental measurements based on the Bayes method [33]. The poloidal mode number ($m = 2$) of this mode is experimentally identified for the first time, which agrees well with the modeling. The mode structure becomes broader as its frequency decreases from 28 kHz (at 334 ms) to 21 kHz (at 340 ms). The broader mode structure leads to stronger redistribution of fast ions, which in turn results in the occurrence of TAE mode as shown in Fig. 1(d).

There can be several alternative interpretations for this low-f mode observed in NSTX. One possible candidate is the ideal peeling mode [34]. However, the peeling mode interpretation cannot explain the observed mode frequency and mode structure in the plasma core. The resistive interchange mode is also unlikely, since the D_R index [35] is usually negative ($D_R < 0$) across the whole plasma column for the studied NSTX cases. A global kink mode, such as the resistive wall mode and/or external kink mode, is easily excluded , since the representative discharge (#138019 at 331 ms) shown below has $\beta_N \approx 2.5$, much below the no-wall beta limit of $\beta_N^{no-wall} \approx 5.2$ computed for this static equilibrium.

The stability scans establish the causal picture: the mode is driven by a finite radial gradient of the centrifugal potential, $\partial(\rho\Omega^2)/\partial R$, arising from either the density or the toroidal-rotation gradient. Instability occurs for $\Omega > \Omega_c\tau_A$, with the density gradient setting the radial location of the mode [Figs. 3(c) and 4]; it disappears when the centrifugal drive vanishes, e.g., for flat density and rotation profiles, or when $\Omega < \Omega_c\tau_A$. A controlled test on equilibrium #137617, removing only the centrifugal-force term while keeping all equilibrium profiles fixed, yields $\gamma\tau_A \leq 0$, confirming that the centrifugal-potential gradient is the essential drive. A pure fluid treatment of the flow-modified equilibrium over-stabilizes the mode, whereas the MHD-kinetic hybrid MARS-K calculation recovers it, reflecting the importance of kinetic parallel-particle dynamics. Other candidate instabilities have already been excluded above.

Conclusion.—Low-frequency modes often observed in the early phase of NSTX discharges are identified as the internal instability, with the dominant poloidal mode number $m = 2$, driven by centrifugal force due to fast toroidal flow. Toroidal modeling recovers most features of the mode as observed in experiments, including (i) the mode frequency; (ii) the synthesized diagnostic data measuring the internal mode structure; (iii) the threshold flow

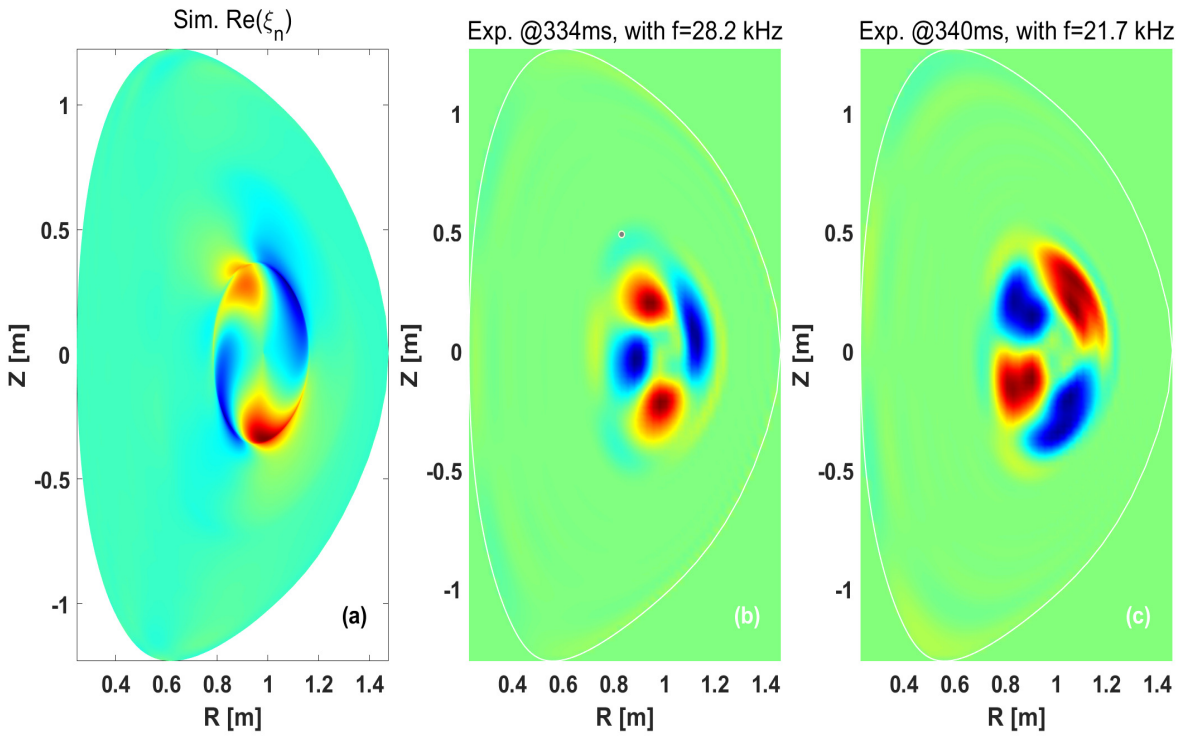


FIG. 7. The comparison of mode structure between simulation and experiment, with (a) the simulated normal displacement in the (R,Z) domain assuming flow modification and kinetic effects, (b,c) the experimental data through Bayesian inversion for 334 and 340 ms in discharge #138019, respectively.

speed $\Omega_c \tau_A$ for the mode onset. Furthermore, it is found that the driving mechanism of the mode is robust against uncertainties in constructing the equilibrium safety factor profile. The mode is located around the location of sharp density gradient. These physics insights into fast flow driven instabilities are crucial not only for interpreting experimental results, but also for developing advanced research plans aimed at high plasma performance in future experiments such as NSTX-U [36] and MAST-U [37]. More importantly, since the achievable rotation value on NSTX is comparable with that for future ST-CTF [1], the results presented here are helpful for the conceptual design of ST reactor to avoid the instabilities driven by fast plasma flow.

[1] Y-K M Peng, P J Fogarty, T W Burgess, D J Strickler *et al.*, Plasma Phys. Control. Fusion

47, B263 (2005).

[2] C. Waldon, S. I. Muldrew, J. Keep, R. Verhoeven, T. Thompson, and M. Kisbey-Ascott, Philosophical Transactions of the Royal Society A: Mathematical, Physical and Engineering Sciences **382**, 20230414 (2024).

[3] H.Reimerdes, A.M. Garofalo, G.L. Jackson, M. Okabayashi,*et. al.*, Phys. Rev. Lett. **98**, 055001 (2007).

[4] J. Berkery, S. Sabbagh, R. Bell, S. Gerhardt, B. LeBlanc, and J. Menard, Nucl. Fusion **55**, 123007 (2015).

[5] J. Luxon, Nucl. Fusion **42**, 614 (2002).

[6] I. Chapman, S. Brown, R. Kemp, and N. Walkden, Nucl. Fusion **52**, 042005 (2012).

[7] M. S. Chu, L. Chen, L.-J. Zheng, C. Ren, and A. Bondeson, Nucl. Fusion **39**, 2107 (1999).

[8] L.-J. Zheng, M. S. Chu, and L. Chen, Phys. Plasmas **6**, 1217 (1999).

[9] P. Helander, R. J. Akers, and L.-G. Eriksson, Phys. Plasmas **12**, 112503 (2005).

[10] M. Ono, S.M. Kaye, Y.-K.M. Peng, G. Barnes *et.al.*, Nucl. Fusion **40**, 557 (2000).

[11] J.E. Menard, R.E. Bell, E.D. Fredrickson, D.A. Gates *et al.*, Nucl. Fusion **45**, 539 (2005).

[12] N. D'Angelo, Phys. Fluids **8**, 1748 (1965).

[13] A. Miura, J. Geophys. Res. Space Physics **89**, 801 (1984).

[14] J. Casanova, J. Jose, E. GarCia-Berro, S. Shore, and A. Calder, Nature **478**, 490 (2011).

[15] S. Munaretto, N. M. Ferraro, and E. D. Fredrickson, Phys. Plasmas **30**, 062502 (2023).

[16] M. Podesta, M. Gorelenkova, D.S. Darrow and E.D. Fredrickson et al., Nucl. Fusion **55**, 053018 (2015).

[17] S.S. Medley, N.N. Gorelenkov, R. Andre, R.E. Bell *et al.*, Nucl. Fusion **44**, 1158 (2004).

[18] J. Yang, M. Podestà, and E. D. Fredrickson, Plasma Phys. Control. Fusion **63**, 045003 (2021).

[19] R.J Goldston, D.C McCune, H.H Towner, S.L Davis *et.al.*, J. Comput. Phys. **43**, 61 (1981).

[20] M. Podesta, M. Gorelenkova, E. D. Fredrickson, N. N. Gorelenkov et al, Phys. Plasmas **23**, 056106 (2016).

[21] J. Menard, R. Bell, E. Fredrickson, D. Gates, S. Kaye, B. LeBlanc, R. Maingi, S. Medley, W. Park, S. Sabbagh, A. Sontag, D. Stutman, K. Tritz, W. Zhu, and the NSTX Research Team, Nucl. Fusion **45**, 539 (2005).

[22] M. S. Chu, J. M. Greene, T. H. Jensen, R. L. Miller, *et al.*, Phys. Plasmas **2**, 2236 (1995).

[23] Y.Q. Liu, A. Bondeson, M.S. Chu, J.-Y. Favez *et al.*, Nucl. Fusion **45**, 1131 (2005).

[24] H. Lutjens, A. Bondeson, and O. Sauter, Comput. Phys. Commun. **97**, 219 (1996).

[25] J.E. Menard, Homepage for the LRDFIT code, http://nstx-u.pppl.gov/software/lrdfit, .

[26] J. W. Berkery, Z. R. Wang, S. A. Sabbagh, Y. Q. Liu, R. Betti, and L. Guazzotto, Phys. Plasmas **24**, 112511 (2017).

[27] S. C. Jardin, N. M. Ferraro, W. Guttenfelder, S. M. Kaye, and S. Munaretto, Phys. Rev. Lett. **128**, 245001 (2022).

[28] S. C. Jardin, N. M. Ferraro, W. Guttenfelder, S. M. Kaye, and S. Munaretto, Phys. Plasmas **30**, 042507 (2023).

[29] D. Stutman, M. Finkenthal, V. Soukhanovskii, M. J. May, H. W. Moos, and R. Kaita, Rev. Sci. Instrum. **70**, 572 (1999).

[30] Y. Q. Liu, M. S. Chu, I. T. Chapman, and T. C. Hender, Phys. Plasmas **15**, 112503 (2008).

[31] J. E. Menard, Z. Wang, Y. Liu, R. E. Bell, S. M. Kaye, J.-K. Park, and K. Tritz, Phys. Rev. Lett. **113**, 255002 (2014).

[32] C. Wahlberg, I. T. Chapman, and J. P. Graves, Phys. Plasmas **16**, 112512 (2009).

[33] D. Li, Y. Liu, J. Svensson, Y. Liu, X. Song, L. Yu, R. Mao, B. Fu, W. Deng, B. Yuan, X. Ji, Y. Xu, W. Chen, Y. Zhou, Q. Yang, X. Duan, Y. Liu, and H.-A. Team, Nucl. Fusion **56**, 036012 (2016).

[34] A.Bortolon et al, 2011,Fast Ion Losses and Redistribution Induced by Low Frequency MHD in NSTX Plasmas, 12th IAEA Technical Meeting on Energetic Particles in Magnetic Confinement Systems,Austin,USA,8-10 September.http://www-naweb.iaea.org/napc/physics/meetings/TM40762.html.

[35] A. Glasser, J. Greene, and J. Johnson, Phys. Fluids **18**, 875 (1975).

[36] S. Munaretto, P. Adebayo-Ige, H. Anand, G. Avdeeva, S. Baek, K. Barada, E. Belli, E. Belova, and J. Berkery, Nucl. Fusion **66**, 035001 (2026).

[37] J. Harrison, A. Aboutaleb, M. Aljunid, S. Allan, R. Allan, A. Alli, H. Anand, Y. Andrew, and L. Appel, Nucl. Fusion **66**, 116005 (2026).

ACKNOWLEDGMENTS

We thank Prof. C. Wahlberg and Prof. M. Hole for very useful discussions and the entire NSTX-U team for their support.

FUNDING DECLARATION

This work was supported by the U.S. DOE under Grant Nos. DE-AC02-09CH11466, DE-FG02-06ER54867, DE-FG03-02ER54681, DE-FG02-95ER54309, DE-FC02-04ER54698, and by National Natural Science Foundation of China (Nos. 11775067, 12375214, 12375232), the National Magnetic Confinement Fusion Energy R&D Program (Nos. 2022YFE03060002 and 2024YFE03200003), and the Nuclear technology research and development program: HJSYF2024(02)-01.

DATA AVAILABILITY

The data that support the findings of this study are available from the corresponding author upon reasonable request.

COMPETING INTERESTS

The authors declare no competing interests.

AUTHOR CONTRIBUTIONS

G.Z.H. and G.Q.D. contributed equally to this work. G.Z.H. performed the experimental analysis, carried out the numerical simulations, and wrote the original draft. G.Q.D. developed part of the code and performed the numerical simulations. Y.Q.L. revealed the underlying physics mechanism. S.X. performed the inversion of the mode structure. W.W.H., E.D.F., J.B., S.M., and K.F.G. provided, analyzed, and interpreted the experimental data. W.L.Z. contributed to the experimental data processing techniques. All authors reviewed and edited the manuscript.